Photocatalytic H_2O_2 production from O_2 under visible light irradiation over phosphate ion-coated Pd nanoparticles-supported $BiVO_4$

Kojiro Fuku[a],*, Ryosuke Takioka[a], Kazushi Iwamura[b], Masanobu Todoroki[b], Kazuhiro Sayama[c], Naoki Ikenaga[a]

[a] *Faculty of Environmental and Urban Engineering, Kansai University, 3-3-35 Yamate-cho, Suita, Osaka 564-8680, Japan.*

[b] *Graduate School of Science and Engineering, Kansai University, 3-3-35 Yamate-cho, Suita, Osaka 564-8680, Japan.*

[c] *Research Center for Photovoltaics (RCPV) and Global Zero Emission Research Center (GZR), National Institute of Advanced Industrial Science and Technology (AIST), Central 5, 1-1-1 Higashi, Tsukuba, Ibaraki 305-8565, Japan.*

* Corresponding author

E-mail address: k.fuku@kansai-u.ac.jp

TEL: +81-6-6368-0894

FAX: +81-6-6388-8869

Abstract

H_2O_2 production from O_2 over Pd nanoparticle (NP) co-catalysts-supported $BiVO_4$ was studied. Several deposition methods and conditions (active metal, co-catalyst loading, solution pH) were investigated for catalyst preparation, and the photo-assisted deposition (PAD) of Pd from an aqueous phosphate buffer solution (pH = 7) was found to be optimal, resulting in small and uniform phosphate ion (PO_4^{3-})-coated Pd NPs being selectively deposited on the reductive surfaces of the $BiVO_4$. This catalyst exhibited better H_2O_2

production from O_2 in the presence of methanol (CH_3OH) as a hole scavenger under visible light irradiation than that by the catalysts prepared by the other methods and under other PAD conditions. It is surmised that PO_4^{3-} partially coats smaller Pd NPs with a narrow size distribution on the reductive surfaces of the $BiVO_4$, and that these NPs promote H_2O_2 generation synergistically by catalyzing the two-electron reduction of O_2 while simultaneously inhibiting the four-electron reduction of O_2 and the two-electron reduction of H_2O_2 to H_2O.

1. Introduction

H_2O_2, which produces only H_2O and/or O_2 on reacting, has been the subject of considerable research attention as a versatile and clean redox agent for selective organic conversions [1-4], environmental purification, bleaching, sterilization and cleaning [5-8], and energy source in H_2O_2 fuel cells [9-13]. H_2O_2 is generally synthesized by the anthraquinone process [14-15]. However, this process suffers a multitude of serious problems, including its multistage nature and reliance on large amounts of harmful organic solvents and H_2. Thus, the development of one-step, H_2-free, aqueous photocatalytic systems to produce H_2O_2 from O_2 [16-26], exploiting inexhaustible light energy, represents a promising strategy to overcome the problems of the anthraquinone process.

In such systems, H_2O_2 is photocatalytically generated by the two-electron reduction of O_2, as shown in Eq. (1):

$$O_2 + 2H^+ + 2e^- \rightarrow H_2O_2 \ (E(O_2/H_2O_2) = +0.68 \text{ V vs. RHE)}) \tag{1}$$
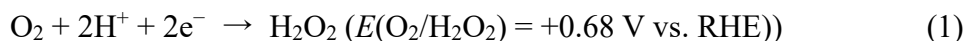
Thus, visible light-responsive photocatalysts capable of driving the O_2 reduction in Eq. (1) are required for the efficient utilization of solar light and thus the realization of economically viable light-driven synthetic processes [18-26]. Encouragingly, several promising examples of materials and systems that produce H_2O_2 effectively from O_2 with H_2O as the electron source (Eqs. 1-3) under visible light or solar light irradiation have been reported [20-26, 33].

$$2H_2O \rightarrow O_2 + 4H^+ + 4e^- \ (E(O_2/H_2O) = +1.23 \text{ V vs. RHE)}) \tag{2}$$

$$2(1) + (2): O_2 + 2H_2O \rightarrow 2H_2O_2 \tag{3}$$
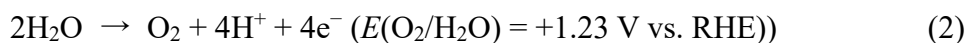
$BiVO_4$ is widely known as an excellent oxide-type photocatalyst having band

potential capable of achieving the reduction of O_2 and the oxidation of H_2O under a wide spectral range of light energy (~520 nm) [26-30]. Accordingly, authors (Fuku and Sayama) have reported the unprecedented production of H_2O_2 from H_2O on a $BiVO_4$ photoanode in aqueous hydrogen carbonate by a two-electron oxidation process under simulated solar light irradiation [31-33]. This anodic reaction was accompanied by H_2O_2 or H_2 production from O_2 or H_2O, respectively, on the cathode. However, although $BiVO_4$ exhibits the unique ability to generate H_2O_2 simultaneously from both O_2 and H_2O under visible light irradiation [33], most previous studies on $BiVO_4$ photocatalysis have focused on application for H_2 production through water splitting rather than through H_2O_2 production.

Au nanoparticles (NPs) are utilized frequently as a reductive co-catalyst to generate H_2O_2 from O_2 on oxide-type photocatalysts [16,18,26,33]. The combination of an Au NP co-catalyst with a $BiVO_4$ photocatalyst has also been reported to facilitate H_2O_2 generation from O_2 and H_2O under visible light or simulated solar light irradiation [26]. Thus, the exploitation of reductive co-catalysts represents a promising strategy to realize the excellent reduction potential of $BiVO_4$ in effective H_2O_2 production through the two-electron reduction of O_2.

Accordingly, in the present study, we investigated optimum metal NPs as a reductive metal co-catalyst for use with $BiVO_4$ in H_2O_2 production from O_2 under visible light irradiation (Fig. 1). Photocatalyst composites were prepared by impregnation (IMP), deposition-precipitation (DP)/chemical reduction (CR) (DP-CR), or photo-assisted deposition (PAD) methods. The catalysts were then characterized thoroughly using X-ray diffractometry (XRD), scanning electron microscopy (SEM), transmission electron

microscopy (TEM), and X-ray photoelectron spectroscopy (XPS), and their performances in the photocatalytic synthesis of H_2O_2 were evaluated.

2. Experimental

2.1. Chemicals

All reagents were commercially available, of reagent grade, and used without further purification.

2.2. Preparation of metal co-catalysts-supported BiVO$_4$

2.2.1 BiVO$_4$ photocatalyst preparation

BiVO$_4$ powder was prepared according to the existing DP method, with a minor change [29-30]. Typically, a suspension of Bi_2O_3 (10 mmol), V_2O_5 (10 mmol), and aqueous 0.5 M HNO_3 (200 mL) was heated at 333 K for 24 h while stirring. After filtration and washing with H_2O, the resulting powder was dried at 60 °C.

2.2.2 Deposition of metal co-catalysts on BiVO$_4$

IMP method: BiVO$_4$ (0.495 g) was added to H_2O (20 mL), and an aqueous solution of the appropriate metal precursor (1.0 wt% (5 mg) in terms of the corresponding zerovalent metal species) was added to the suspension. After the suspension was evaporated at 333 K under vacuum, the obtained powder was dried at 383 K for 1 h and then calcined at 723 K for 2 h. An aqueous solution of $HAuCl_4$, $IrCl_4$, $RuCl_3$, $RhCl_3$, $AgNO_3$, H_2PtCl_6, $(NH_4)_2[PdCl_4]$, $MnCl_2$, $NiCl_2$, $CoCl_2$, or $CuCl_2$ was used as the metal precursor. In addition, 0.1 and 0.5 wt% Pd catalysts were also prepared using the same procedure, except with different concentrations of the aqueous $(NH_4)_2[PdCl_4]$ precursor.

DP-CR method: The deposition of Pd onto the BiVO$_4$ by DP-CR was performed

by reference to the existing literature of DP and CR methods [34-36]. Briefly, $BiVO_4$ (0.495 g) was added to H_2O (50 mL), and then an aqueous solution of $(NH_4)_2[PdCl_4]$ (1 wt% (5 mg) in terms of Pd^0) was added to the suspension. The pH of the suspension was adjusted to 11 by the addition of 28% aqueous NH_3, and the suspension was heated to reflux for 2 h while stirring. To reduce the Pd species, an aqueous solution of $NaBH_4$ was added to the suspension ($Pd:NaBH_4 = 1:100$ (mol/mol)), and the suspension was heated to reflux for a further 1 h while stirring. After filtration and washing with H_2O, the resulting powder was dried at 60 °C.

PAD method (with and without phosphate): $BiVO_4$ (0.495 g) was suspended in an aqueous solution (100 mL) containing 10 vol% CH_3OH as a hole scavenger with or without phosphate buffer solution (90 mM) adjusted to pH = 5.1, 7.2, 8.9, or 10.9. Then, an aqueous solution of $(NH_4)_2[PdCl_4]$ (1 wt% (5 mg) in terms of Pd^0) was added to the suspension. The suspension was photo-irradiated at $\lambda > 300$ nm with a 300-W Xe illuminator (ILC Technology, Inc., CERMAX LX-300) while stirring under ambient pressure in an ice bath for 2 h. After filtration and washing with H_2O, the resulting powder was dried at 60 °C. The pH of the phosphate solution was adjusted by changing the amounts of Na_2HPO_4, NaH_2PO_4, and NaOH therein. $BiVO_4$ catalysts with Pd loadings of 0.01, 0.05, 0.1, and 0.5 wt% were also prepared by the same procedure, except with different concentrations of aqueous $(NH_4)_2[PdCl_4]$. For comparison, preparation of other $BiVO_4$ photocatalysts with Pd loadings of 0.1 wt% by the PAD method was also performed by the same procedure, except with substituting aqueous borate, acetate, carbonate, and citrate buffer solutions adjusted to pH = *ca.* 7 for the phosphate solution.

2.3. Characterization

Catalysts were characterized using XRD (SmartLab, Rigaku, Ltd.) with monochromatic Cu-Kα radiation, SEM (S-4800, Hitachi, Ltd.), TEM (JEM-2010, JEOL, Ltd.), and XPS (JPS-9010MX, JEOL, Ltd.) with Mg-Kα radiation.

2.4. H_2O_2 production from O_2 over metal co-catalysts-supported $BiVO_4$

A prepared photocatalyst sample was suspended in H_2O (45 mL) in a test tube ($\phi 30 \times 200$ mm). After the test tube was bubbled with O_2 for 15 min at 200 mL min^{-1} in an ice bath, CH_3OH (5 mL) as hole scavenger was added to the suspension while O_2 bubbling. The suspension was bubbled with O_2 for further 5 min and sealed with a silicone stopper. The test tube was photo-irradiated in an ice bath for 2 h at $\lambda > 420$ nm using a 300-W Xe illuminator equipped with a cut-off filter (HOYA Corp., L42). The concentration of H_2O_2 generated was measured by colorimetry based on the color change of Fe^{2+} to Fe^{3+} [31-33] using a UV–vis spectrophotometer (PD-3500UV, APEL Co., Ltd.). Briefly, 0.1 mL of 0.1 M $FeSO_4$ in 0.5 M aqueous H_2SO_4 solution was added to a solution containing 1.0 mL of reaction sample and 0.9 mL of 0.5 M aqueous H_2SO_4 solution. The H_2O_2 concentration was measured by Fe^{3+} colorimetry (305 nm).

3. Results and discussion

3.1. Effects of metal species and co-catalyst preparation method

H_2O_2 production from O_2 in the presence of CH_3OH as a hole scavenger under visible light ($\lambda > 420$ nm) irradiation using different metal co-catalysts (1 wt%)-supported $BiVO_4$ prepared using the IMP method is shown in Fig. 2. Almost all the metal-bearing catalysts exhibited higher H_2O_2 generation performances than that of bare $BiVO_4$ (except for supported Ir and Mn), and the performances increased in the order Ni $\doteqdot$ Co < Ru <

Rh < Ag < Cu ≐ Pt << Pd. Pt being known to promotes electrochemical H_2O generation by the four-electron reduction of O_2 and the two-electron reduction of H_2O_2 [37-38], and Cu as base metal species facilitated H_2O_2 production from O_2 well under these reaction conditions. It should also be noted that Pd was by far the most effective co-catalyst for H_2O_2 production from O_2, exhibiting a performance that was *ca.* 9.3 times greater than that of Au, which is a conventional co-catalyst to generate H_2O_2 from O_2. It has also been reported that Au requires a higher overpotential for the electrochemical reduction of O_2 than those of Pt or Pd, and that Pt exhibits higher activity at lower overpotentials in the four-electron reduction of O_2 than that for Pd [37-38]. This results in poorer performances in terms of reactivity and selectivity in H_2O_2 generation *via* the two-electron reduction of O_2 for Au and Pt, respectively. In this study also, the specific improvement of performance by Pd supported on the $BiVO_4$ photocatalyst might be caused by both a comparatively low overpotential and a high selectivity for the two-electron reduction of O_2.

For the Pd co-catalyst, the effects of the preparation method on performance were also investigated using the conventional methods of IMP and DP-CR as well as the PAD method (Fig. 3). As shown in Fig. 3(A), XRD patterns derived from the monoclinic structure, which exhibits higher photocatalytic activity in H_2O splitting than other $BiVO_4$ crystal forms [29-30], were observed for bare $BiVO_4$, and this structure was maintained after the deposition of Pd NPs by IMP and PAD. However, peaks for Bi metal were observed for the catalyst prepared by the DP-CR method, suggesting that some $BiVO_4$ was reduced to Bi^0 by the $NaBH_4$ used as a reducing agent in the chemical reduction. Moreover, no diffraction peaks ascribed to Pd NPs were observed for any of the samples, suggesting that the Pd NPs supported on the $BiVO_4$ were highly dispersed.

In addition, the $BiVO_4$ prepared in this study possesses a unique decahedral structure with separate sites (faces) for reduction and oxidation reactions, and it has been demonstrated previously by observing these deposition sites using the photo-deposition method of metals or metal oxides and from a difference in energy levels of {010} and {110} facets calculated by DFT that the two facets on the top and bottom (the {010} faces) and the eight side facets (the {110} faces) act as reduction and oxidation sites, respectively (Fig. 3(B)(a)) [39]. As seen in the SEM images shown in Fig. 3(B)(b), the IMP method provided Pd NPs with sizes of 20–70 nm, distributed randomly over the entire $BiVO_4$ surface. In addition, the DP-CR method provided Pd-$BiVO_4$ having distinctly different patterned indented surface structure over the entire $BiVO_4$ surface compared with other samples. From the XRD pattern of Fig. 3(A)(c), it indicated that the patterned indented surface structure was formed by composite particles of Pd species and Bi^0 derived from the $BiVO_4$ by the chemical reduction. Conversely, the catalysts prepared using the PAD method (without phosphate) showed agglomerations of Pd NPs with sizes of 10–60 nm supported selectively on the reductive surfaces ({010} faces) of the $BiVO_4$ (Fig. 3(B)(d)), indicating that the Pd species were reductively supported by the action of excited electrons generated on the reductive surfaces under light irradiation.

Figure 3(C) shows a comparison of the H_2O_2 production performances achieved using these Pd-$BiVO_4$ catalysts. Pd-$BiVO_4$ prepared using the DP-CR method exhibited very poor H_2O_2 production properties, in that the photocatalytic activity was lost due to the reduction of $BiVO_4$ discussed above or inhibiting H_2O_2 generation over the Pd-$BiVO_4$ by generating Bi^0. Interestingly, the Pd-$BiVO_4$ prepared by the PAD method without aqueous buffer solution exhibited a H_2O_2 production performance *ca.* 2.1 times better

than that prepared by the IMP method.

The effects of Pd loading on H_2O_2 generation for catalysts prepared by the IMP and PAD methods were also investigated, as shown in Fig. 4. In both cases, the performance decreased significantly with increasing loading in the range 0.1–1.0 wt%, and the performance of Pd-BiVO$_4$ prepared using the PAD method without aqueous buffer solution was maximal at *ca.* 340 μM. From the SEM images of 0.1 and 1.0 wt% Pd-BiVO$_4$ prepared by the PAD method without aqueous buffer solution (Fig. S1), better dispersed and smaller Pd NPs were observed clearly for a Pd loading of 0.1 wt% than those observed for a Pd loading of 1.0 wt%. The results shown in Figs. 3, 4, and S1 indicate that smaller Pd NPs supported selectively on the reductive surfaces of the BiVO$_4$ facilitate H_2O_2 production from O_2.

3.2. Effects of PAD conditions

The pH of the solvent employed in PAD significantly affects the size of the resultant NPs supported on the photocatalytic support [40], meaning that smaller Pd NPs can be deposited on the reductive surfaces of BiVO$_4$ by performing PAD under optimal pH conditions. Accordingly, to improve the H_2O_2 production performance of Pd-BiVO$_4$ prepared by the PAD method, we focused on optimizing the deposition conditions.

In this study, a phosphate buffer solution was used as a pH adjuster as a means to maintain a fixed pH during PAD. Fig. 5 shows the H_2O_2 production performance from O_2 of 0.1 wt% Pd-BiVO$_4$ prepared using the PAD method with phosphate solutions adjusted to different pH values ranging from acidic to basic. The performance changed significantly with the pH and the maximum performance was achieved for pH = 7.2, where the maximum accumulation reached *ca.* 600 μM after only 2 h. This was *ca.* 1.8

times greater than that for 0.1 wt% Pd-BiVO$_4$ prepared using the PAD method without pH adjustment.

To identify the specific factors responsible for this pH-dependent performance, the average particle sizes (d_{av}) and size distributions of the Pd NPs were obtained from TEM images of the samples prepared at pH = 3.5 (without pH adjustment), 7.2, and 10.9 (Fig. 6). The d_{av} and size distributions of the Pd NPs clearly changed significantly with the pH. The sample prepared at pH = 7.2 presented the lowest d_{av} and narrowest size distribution of Pd NPs of the samples analyzed (Fig. 6(b)). On the other hand, the Pd NPs deposited at pH = 10.9 presented a particularly wide size distribution and the highest d_{av}.

It has been reported that (NH$_4$)$_2$[PdCl$_4$], used in this study as a Pd precursor, undergoes changes in coordination geometry with the changing pH of the solution [41-42]. The Cl$^-$ in the [PdCl$_4$]$^{2-}$ is substituted gradually by OH$^-$ on increasing the pH beyond 6 [41], and [PdCl(H$_2$O)$_3$]$^+$ and [PdCl$_2$(H$_2$O)$_2$] complexes are formed at pH < 3.8 [42]. Based on these results and those of previous reports, the [PdCl$_x$(OH)$_{4-x}$]$^{2-}$ complex formed at pH = 7.2 is better suited to the deposition of highly dispersed, small, narrow size distribution Pd NPs by the PAD method compared with the [PdCl(H$_2$O)$_3$]$^+$/[PdCl$_2$(H$_2$O)$_2$] or [PdCl(OH)$_3$]$^{2-}$/[Pd(OH)$_4$]$^{2-}$ complexes that are expected to form at pH = 3.5 or 10.9, respectively. In addition, these results also indicate that smaller Pd NPs supported on the BiVO$_4$ improve reductive H$_2$O$_2$ production from O$_2$. It has also been reported that the amount of electrons (*i.e.*, negative charge state) trapped in Au NPs supported on a Si wafer increases proportionately with increasing particle size [43]. This suggests that, in the present study, increasing the particle size of the Pd NPs would lead to better performance for multielectron reduction processes, *i.e.*, the

unfavorable four-electron reduction of O_2 to H_2O (the back reaction of Eq. (2)), resulting in a decreasing selectivity for H_2O_2 generation by the two-electron reduction of O_2. Thus, smaller Pd NPs supported on the reductive surfaces of the $BiVO_4$ would act as an excellent co-catalyst for H_2O_2 production by the two-electron reduction of O_2 rather than the four-electron reduction of O_2, resulting in significant different co-catalyst performances of Pd NPs prepared at pH = 7.2 and 10.9 with phosphate.

On the other hand, although Pd NPs prepared at pH = 3.5 without phosphate exhibited a higher abundance rate of smaller NPs (< 10 nm) than that prepared at pH = 10.9 with phosphate (Figs. 6(a) and (c)), low H_2O_2 production performance was confirmed equivalent to that on the sample prepared at pH = 10.9 with phosphate possessing a bigger d_{av} and a wider distribution of Pd NPs. These results may indicate that "phosphate" utilized as the pH adjuster in the PAD also facilitates H_2O_2 production intrinsically from O_2.

To fully investigate the effects of phosphate on H_2O_2 production from O_2 (other than those related to its role as a pH adjuster), 0.1 wt% Pd-$BiVO_4$ catalysts were prepared using PAD at pH = *ca.* 7 from aqueous solutions containing buffer species other than phosphate. As shown in Fig. 7, although a pH of 7 was used for all the depositions, the performance changed significantly depending on the species used in the aqueous buffer solution. In the case of using citrate, citrate ions might be adsorbed strongly onto the Pd NPs, even after PAD, resulting in a decrease in the occurrence of the two-electron O_2 reduction. Indeed, there are many reports of citrate ions acting as a reducing agent and/or aggregation inhibitor in metallic NP preparation by the chemical reduction method [44-45]. Conversely, 0.1 wt% Pd-$BiVO_4$ prepared using acetate, carbonate, and borate

exhibited higher performance than that prepared without the buffer, but their effects were clearly lower than those observed for the phosphate buffer.

The TEM image of 0.1 wt% Pd-BiVO$_4$ prepared using carbonate (Fig. S2(a)), which exhibited the lowest performance other than that prepared using citrate, revealed that the d$_{av}$ and size distribution for these Pd NPs were similar to those for the NPs prepared using phosphate. These results (Figs. 7 and S2) demonstrate clearly that the phosphate contributes to H$_2$O$_2$ production from O$_2$ through effects other than those as simply a pH buffering agent.

3.3. Mechanism of the effect of phosphate on Pd-BiVO$_4$ performance

To investigate the specific effects of phosphate ions on H$_2$O$_2$ production from O$_2$, Pd(3d) and P(2p) XPS spectra were obtained from Pd-BiVO$_4$ prepared at pH = 7.2 using phosphate solution (Fig. 8(A) and (B)). A catalyst loading of 1.0 wt% Pd was used for confirming the information of Pd NPs in detail. For comparison, a sample of BiVO$_4$ photo-irradiated in an ice bath for 2 h at λ > 300 nm using a 300-W Xe illuminator in phosphate solution adjusted to pH = 7.2 without (NH$_4$)$_2$[PdCl$_4$] was also obtained (Fig. 8(C)).

Interestingly, the presence of both Pd and P species on the surface of the 1.0 wt% Pd-BiVO$_4$ was confirmed. In the Pd(3d$_{5/2\ and\ 3/2}$) spectra, the 1.0 wt% Pd-BiVO$_4$ presented two peaks at 337.9 eV and 343.3 eV due to tetravalent Pd oxide (PdO$_2$) (Fig. 8(A)) [46-47], although the Pd NPs were supported on the reductive surfaces of the BiVO$_4$ using the PAD method. It has also been known that surface of reduced Pd species is easily oxidized in the presence of O$_2$ [48-49]. In this study also, surface oxide layer of the PdO$_2$ might be formed by the O$_2$, after the Pd species were reductively supported on the

reductive surfaces under light irradiation. In the P($2p_{3/2 \text{ and } 1/2}$) spectra, two peaks at 133.0 eV and 134.3 eV due to phosphate ions (PO_4^{3-}) were observed. (Fig. 8(B)) [50-52]. Furthermore, no peaks due to bonds between Pd and P (such as those in Pd-P and Pd-PO) were observed in the Pd(3d) and P(2p) spectra. In addition, no spectrum was confirmed in the XPS measurements of P(2p) on the $BiVO_4$-irradiated visible light in the same procedure other than using aqueous buffer solutions of phosphate at pH = 7.2 without $(NH_4)_2[PdCl_4]$ as the Pd precursor in the PAD method (Fig. 8(C)). These results suggest that PO_4^{3-} partially coated only on the Pd NPs, not on the $BiVO_4$, by the PAD method using phosphate (Fig. 8).

It is noted that phosphate is widely known to be an effective stabilizer of H_2O_2 [53]. To confirm the effect of phosphate on H_2O_2 degradation during the reaction, reductive H_2O_2 production from O_2 in an aqueous solution of CH_3OH containing H_2O_2 (200 μM) was also performed using 0.1 wt% Pd-$BiVO_4$ prepared at pH = *ca.* 7 using aqueous carbonate or phosphate buffer solutions (Fig. 9). The amount of H_2O_2 generated decreased with the initial addition of H_2O_2 in both cases, suggesting that the H_2O_2 generated was consumed during the reaction between H_2O_2 and the carriers generated by $BiVO_4$ photocatalysis (excited electrons or holes). However, the decrease in the rate of H_2O_2 generation over 0.1 wt% Pd-$BiVO_4$ prepared using phosphate was *ca.* 31%, whereas that for carbonate was *ca.* 58%. In addition, degradation test of H_2O_2 (1 mM) in an aqueous solution of CH_3OH under condition of Ar (oxygen-free) atmosphere that cannot generate H_2O_2 was also performed in the absence or presence of visible light (λ > 420 nm). As shown in Fig. S3, the degradation of H_2O_2 over 0.1 wt% Pd-$BiVO_4$ prepared using phosphate was significantly inhibited compared with that for carbonate in both conditions

of dark and light irradiation. These results suggest that the PO_4^{3-} partially coated Pd NPs act as effective co-catalyst for selective reduction of O_2 to H_2O_2 by inhibiting H_2O_2 degradation (Fig. 10). As shown in proposed mechanism of Fig. 10, the results suggested that a $BiVO_4$ photocatalyst decorated selectively on its reductive faces with small, narrow size distribution, partially phosphate-coated Pd NPs exhibited excellent activity for H_2O_2 production from O_2.

4. Conclusions

In summary, the Pd was suitable metal co-catalyst for H_2O_2 production by the two-electron reduction of O_2 under visible light ($\lambda > 420$ nm) irradiation on the $BiVO_4$ photocatalyst. The PAD method using an aqueous phosphate buffer solution adjusted at pH = 7.2 provided smaller Pd NPs with a narrow size distribution on the reductive surfaces of the $BiVO_4$ photocatalyst compared with the conventional methods of IMP and DP-CR and other conditions in the PAD method. The 0.1 wt% Pd-$BiVO_4$ prepared in the PAD method using phosphate achieved the maximum performance, where the maximum accumulation reached *ca.* 600 μM after only 2 h, in our tried photocatalysts in this study. The specific improvement of performance might be concluded to be a result of the synergy by the formation of small Pd NPs on the reductive surfaces of the $BiVO_4$ in the PAD at pH = 7 and partial PO_4^{3-} coat on Pd NPs derived from the phosphate. This study contributes to the developing design guidelines of promising co-catalyst for achieving efficient H_2O_2 generation and accumulation from O_2. The more detail tracking of Pd species for improving the H_2O_2 generation and inhibiting the degradation of H_2O_2, and oxidative and reductive H_2O_2 production from H_2O and O_2 using the Pd-$BiVO_4$ are the

subjects of current investigations.

Declaration of Competing Interest

The authors declare no conflict of interest.

References

[1] R. Noyori, M. Aoki, K. Sato, Green oxidation with aqueous hydrogen peroxide, Chem. Commun. (2003) 1977-1986.

[2] Y. Kon, S. Tanaka, K. Sato, Clean and practical oxidation using hydrogen peroxide–Development of catalysis and application to fine chemicals–, Synthesiology 8 (2015) 15-26.

[3] A. Fingerhut, O. V. Serdyuk, S. B. Tsogoeva, Non-heme iron catalysts for epoxidation and aziridination reactions of challenging terminal alkenes: towards sustainability, Green Chem. 17 (2015) 2042-2058.

[4] H. Yamashita, K. Mori, Y. Kuwahara, T. Kamegawa, M. Wen, P. Verma, M. Che, Single-site and nano-confined photocatalysts designed in porous materials for

environmental uses and solar fuels, Chem. Soc. Rev. 47 (2018) 8072-8096.

[5] Y. Zhu, R. Zhu, Y. Xi, J. Zhu, G. Zhu, H. He, Strategies for enhancing the heterogeneous Fenton catalytic reactivity: A review, Appl. Catal. B: Environ. 255 (2019) 117739.

[6] A. Sorokin, S. D. Suzzoni-Dezard, D. Poullain, J. P. Noël, B. Meunier, CO_2 as the ultimate degradation product in the H_2O_2 oxidation of 2,4,6-Trichlorophenol catalyzed by iron tetrasulfophthalocyanine, J. Am. Chem. Soc. 118 (1996) 7410-7411.

[7] Y. Wu, J. Wu, F. Yang, C. Tang, Q. Huang, Effect of H_2O_2 bleaching treatment on the properties of finished transparent wood, Polymers 11 (2019) 776.

[8] R. Armon, N. Laot, O. Lev, H. Shuval, B. Fattal, Controlling biofilm formation by hydrogen peroxide and silver combined disinfectant, Water Sci. Technol. 42 (2000) 187-192.

[9] Y. Yang, R. Dong, Y. Zhu, H. Li, H. Zhang, X. Fan, H. Chang, High-performance direct hydrogen peroxide fuel cells (DHPFCs) with silver nanowire-graphene hybrid aerogel as highly-conductive mesoporous electrodes, Chem. Eng. J. 381 (2020) 122749.

[10] M. H. Tran, B. J. Park, B. H. Kim, H. H. Yoon, Mesoporous silica template-derived nickel-cobalt bimetallic catalyst for urea oxidation and its application in a direct urea/H_2O_2 fuel cell, Int. J. Hydrogen Energy 45 (2020) 1784-1792.

[11] S. A. M. Shaegh, S. M. M. Ehteshami, S. H. Chan, N. T. Nguyen, S. N. Tan, Membraneless hydrogen peroxide micro semi-fuel cell for portable applications, RSC Adv. 4 (2014) 37284-37287.

[12] Y. Yamada, M. Yoneda, S. Fukuzumi, High and robust performance of H_2O_2 fuel

cells in the presence of scandium ion, Energy Environ. Sci. 8 (2015) 1698-1701.

[13] K. Mase, M. Yoneda, Y. Yamada, S. Fukuzumi, Seawater usable for production and consumption of hydrogen peroxide as a solar fuel, Nature Commun. 7 (2016) 11470.

[14] X. Jia, F. Sun, Y. Fei, M. Jin, F. Zhang, W. Xu, N. Shi, Z. Lv, Explosion characteristics of mixtures containing hydrogen peroxideand working solution in the anthraquinone route to hydrogen peroxide, Process Saf. Environ. Prot. 119 (2018) 218-222.

[15] S. Ranganathan, V. Sieber, Recent advances in the direct synthesis of hydrogen peroxide using chemical catalysis–A review, Catalysts 8 (2018) 379.

[16] M. Teranishi, S. Naya, H. Tada, Temperature- and pH-dependence of hydrogen peroxide formation from molecular oxygen by gold nanoparticle-loaded titanium(IV) oxide photocatalyst, J. Phys. Chem C 120 (2016) 1083-1088.

[17] B. O. Burek, D. W. Bahnemann, J. Z. Bloh, Modeling and optimization of the photocatalytic reduction of molecular oxygen to hydrogen peroxide over titanium dioxide, ACS Catal. 9 (2019) 25-37.

[18] M. Teranishi, R. Hoshino, S. Naya, H. Tada, Gold-nanoparticle-loaded carbonate-modified titanium(IV) oxide surface: Visible-light-driven formation of hydrogen peroxide from oxygen, Angew. Chem. Int. Ed. 55 (2016) 12773-12777.

[19] H. Kim, O. S. Kwon, S. Kim, W. Choi, J. H. Kim, Harnessing low energy photons (635 nm) for the production of H_2O_2 using upconversion nanohybrid photocatalysts, Energy Environ. Sci. 9 (2016) 1063-1073.

[20] Y. Shiraishi, S. Kanazawa, Y. Kofuji, H. Sakamoto, S. Ichikawa, S. Tanaka, T. Hirai, Sunlight-driven hydrogen peroxide production from water and molecular

oxygen by metal-free photocatalysts, Angew. Chem. Int. Ed. 53 (2014) 13454-13459.

[21] Y. Kofuji, S. Ohkita, Y. Shiraishi, H. Sakamoto, S. Tanaka, S. Ichikawa, T. Hirai, Graphitic carbon nitride doped with biphenyl diimide: Efficient photocatalyst for hydrogen peroxide production from water and molecular oxygen by sunlight, ACS Catal. 6 (2016) 7021-7029.

[22] Y. Kofuji, Y. Isobe, Y. Shiraishi, H. Sakamoto, S. Ichikawa, S. Tanaka, T. Hirai, Hydrogen peroxide production on a carbon nitride-boron nitride-reduced graphene oxide hybrid photocatalyst under visible light, ChemCatChem 10 (2018) 2070-2077.

[23] Y. Shiraishi, T. Takii, T. Hagi, S. Mori, Y. Kofuji, Y. Kitagawa, S. Tanaka, S. Ichikawa, T. Hirai, Resorcinol–formaldehyde resins as metal-free semiconductor photocatalysts for solar-to-hydrogen peroxide energy conversion, Nature Mater. 18 (2019) 985-993.

[24] S. Fukuzumi, Y. M. Lee, W. Nam, Photocatalytic oxygenation reactions using water and dioxygen, ChemSusChem 12 (2019) 3931-3940.

[25] Y. H. Hong, J. W. Han, J. Jung, T. Nakagawa, Y. M. Lee, W. Nam, S. Fukuzumi, Photocatalytic oxygenation reactions with a cobalt porphyrin complex using water as an oxygen source and dioxygen as an oxidant, J. Am. Chem. Soc. 141 (2019) 9155-9159.

[26] H. Hirakawa, S. Shiota, Y. Shiraishi, H. Sakamoto, S. Ichikawa, T. Hirai, Au nanoparticles supported on $BiVO_4$: Effective inorganic photocatalysts for H_2O_2 production from water and O_2 under visible light, ACS Catal. 6 (2016) 4976-4982.

[27] A. Kudo, K. Ueda, H. Kato, I. Mikami, Photocatalytic O_2 evolution under visible

light irradiation on BiVO$_4$ in aqueous AgNO$_3$ solution, Catal. Lett. 53 (1998) 229-230.

[28] K. Sayama, A. Nomura, Z. Zou, R. Abe, Y. Abe, H. Arakawa, Photoelectrochemical decomposition of water on nanocrystalline BiVO$_4$ film electrodes under visible light, Chem. Commun. (2003) 2908-2909.

[29] A. Iwase, A. Kudo, Photoelectrochemical water splitting using visible-light-responsive BiVO$_4$ fine particles prepared in an aqueous acetic acid solution, J. Mater. Chem. 20 (2010) 7536-7542.

[30] Y. Miseki, K. Sayama, Highly efficient Fe(III) reduction and solar-energy accumulation over a BiVO$_4$ photocatalyst, Chem. Commun. 54 (2018) 2670-2673.

[31] K. Fuku, K. Sayama, Efficient oxidative hydrogen peroxide production and accumulation in photoelectrochemical water splitting using a tungsten trioxide/bismuth vanadate photoanode, Chem. Commun. 52 (2016) 5406-5409.

[32] K. Fuku, Y. Miyase, Y. Miseki, T. Gunji, K. Sayama, WO$_3$/BiVO$_4$ photoanode coated with mesoporous Al$_2$O$_3$ layer for oxidative production of hydrogen peroxide from water with high selectivity, RSC Adv. 7 (2017) 47619-47623.

[33] K. Fuku, Y. Miyase, Y. Miseki, T. Funaki, T. Gunji, K. Sayama, Photoelectrochemical hydrogen peroxide production from water on a WO$_3$/BiVO$_4$ photoanode and from O$_2$ on an Au cathode without external bias, Chem. Asian J. 12 (2017) 1111-1119.

[34] B. Tapin, F. Epron, C. Especel, B. K. Ly, C. Pinel, M. Besson, Study of monometallic Pd/TiO$_2$ catalysts for the hydrogenation of succinic acid in aqueous phase, ACS Catal. 3 (2013) 2327-2335.

[35] A. L. Bugaev, V. A. Polyakov, A. A. Tereshchenko, A. N. Isaeva, A. A. Skorynina, E. G. Kamyshova, A. P. Budnyk, T. A. Lastovina, A. V. Soldatov, Chemical synthesis and characterization of Pd/SiO_2: The effect of chemical reagent, Metals 8 (2018) 135.

[36] Y. Holade, C. Canaff, S. Poulin, T. W. Napporn, K. Servat, K. B. Kokoh, High impact of the reducing agent on palladium nanomaterials: new insights from X-ray photoelectron spectroscopy and oxygen reduction reaction, RSC Adv. 6 (2016) 12627-12637.

[37] S. Siahrostami, A. Verdaguer-Casadevall, M. Karamad, D. Deiana, P. Malacrida, B. Wickman, M. Escudero-Escribano, E. A. Paoli, R. Frydendal, T. W. Hansen, I. Chorkendorff, I. E. L. Stephens, J. Rossmeisl, Enabling direct H_2O_2 production through rational electrocatalyst design, Nature Mater. 12 (2013) 1137-1143.

[38] A. Verdaguer-Casadevall, D. Deiana, M. Karamad, S. Siahrostami, P. Malacrida, T. W. Hansen, J. Rossmeisl, I. Chorkendorff, I. E. L. Stephens, Trends in the electrochemical synthesis of H_2O_2: Enhancing activity and selectivity by electrocatalytic site engineering, Nano Lett. 14 (2014) 1603-1608.

[39] R. Li, F. Zhang, D. Wang, J. Yang, M. Li, J. Zhu, X. Zhou, H. Han, C. Li, Spatial separation of photogenerated electrons and holes among {010} and {110} crystal facets of $BiVO_4$, Nature Commun. 4 (2013) 1432.

[40] V. Iliev, D. Tomova, L. Bilyarska, G. Tyuliev, Influence of the size of gold nanoparticles deposited on TiO_2 upon the photocatalytic destruction of oxalic acid, J. Mol. Catal. A: Chem. 263 (2007) 32-38.

[41] J. J. Cruywagen, R. J. Kriek, Complexation of palladium(II) with chloride and

hydroxide, J. Coord. Chem. 60 (2007) 439-447.

[42] G. Agostini, E. Groppo, A. Piovano, R. Pellegrini, G. Leofanti, C. Lamberti, Preparation of supported Pd catalysts: From the Pd precursor solution to the deposited Pd^{2+} phase, Langmuir 26 (2010) 11204-11211.

[43] Y. Zhang, O. Pluchery, L. Caillard, A. F. Lamic-Humblot, S. Casale, Y. J. Chabal, M. Salmeron, Sensing the charge state of single gold nanoparticles via work function measurements, Nano Lett. 15 (2015) 51-55.

[44] D. Curry, A. Cameron, B. MacDonald, C. Nganou, H. Scheller, J. Marsh, S. Beale, M. Lu, Z. Shan, R. Kaliaperumal, H. Xu, M. Servos, C. Bennett, S. MacQuarrie, K. D. Oakes, M. Mkandawirea, X. Zhang, Adsorption of doxorubicin on citrate-capped gold nanoparticles: insights into engineering potent chemotherapeutic delivery systems, Nanoscale 7 (2015) 19611-19619.

[45] H. E. Toma, V. M. Zamarion, S. H. Toma, K. Araki, The coordination chemistry at gold nanoparticles, J. Braz. Chem. Soc. 21 (2010) 1158-1176.

[46] B. Qi, L. Di, W. Xu, X. Zhang, Dry plasma reduction to prepare a high performance Pd/C catalyst at atmospheric pressure for CO oxidation, J. Mater. Chem. A 2 (2014) 11885-11890.

[47] H. U. Shin, D. Lolla, Z. Nikolov, G. G. Chase, Pd–Au nanoparticles supported by TiO_2 fibers for catalytic NO decomposition by CO, J. Ind. Eng. Chem. 33 (2016) 91-98.

[48] B. Brandt, T. Schalow, M. Laurin, S. Schauermann, J. Libuda, H.-J. Freund, Oxidation, reduction, and reactivity of supported Pd nanoparticles: Mechanism and Microkinetics, J. Phys. Chem. C 111 (2007) 938-949.

[49] K. Shimizu, T. Kubo, A. Satsuma, Surface oxygen-assisted Pd nanoparticle catalysis for selective oxidation of silanes to silanols, Chem. Eur. J. 18 (2012) 2226-2229.

[50] Y. C. Lin, Y. Y. Chen, B. Y. Yu, W. C. Lin, C. H. Kuo, J. J. Shyue, Sputter-induced chemical transformation in oxoanions by combination of C_{60}^+ and Ar^+ ion beams analyzed with X-ray photoelectron spectrometry, Analyst 134 (2009) 945-951.

[51] Y. Liu, Y. Zhou, J. Zhang, Y. Xia, T. Chen, S. Zhang, Monoclinic phase $Na_3Fe_2(PO_4)_3$: Synthesis, structure, and electrochemical performance as cathode material in sodium-ion batteries, ACS Sustainable Chem. Eng. 5 (2017) 1306-1314.

[52] S. Wang, H. Xu, W. Li, A. Dolocan, A. Manthiram, Interfacial chemistry in solid-state batteries: Formation of interphase and its consequences, J. Am. Chem. Soc. 140 (2018) 250-257.

[53] N. H. Kim, J. H. Lim, S. Y. Kim, E. G. Chang, Effects of phosphoric acid stabilizer on copper and tantalum nitride CMP, Mater. Lett. 57 (2003) 4601-4604.
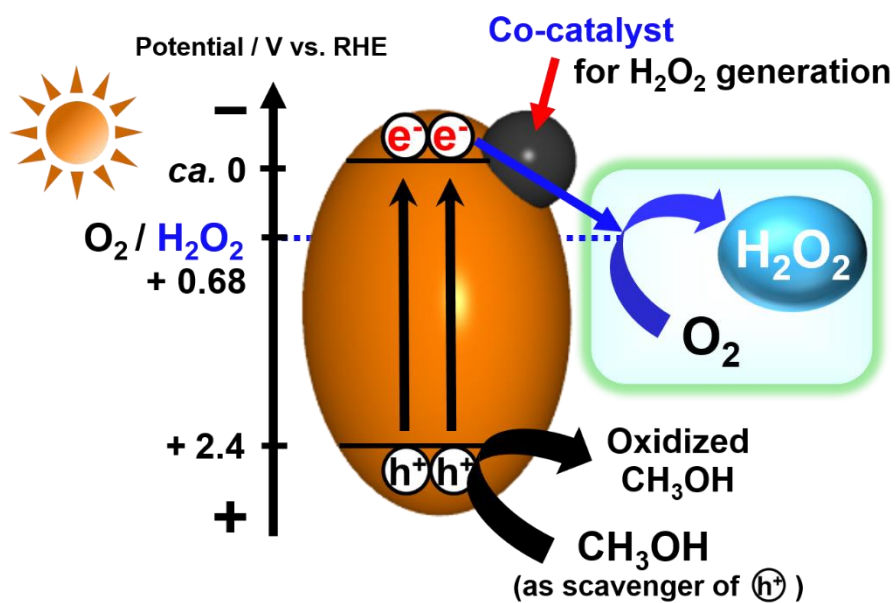
Fig. 1. Schematic of photocatalytic H_2O_2 generation from O_2 over a reductive co-catalyst-supported $BiVO_4$ in the presence of CH_3OH as a hole scavenger.
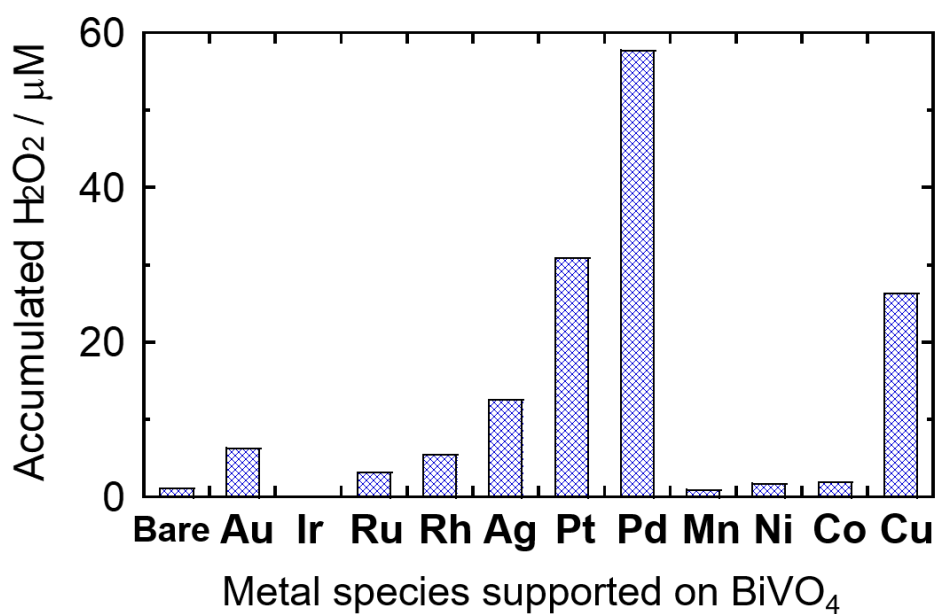
Fig. 2. Effects of metal co-catalyst species (1 wt%) supported on BiVO$_4$ using the IMP method on H$_2$O$_2$ production from O$_2$ in the presence of CH$_3$OH under visible light (λ > 420 nm) irradiation for 2 h.
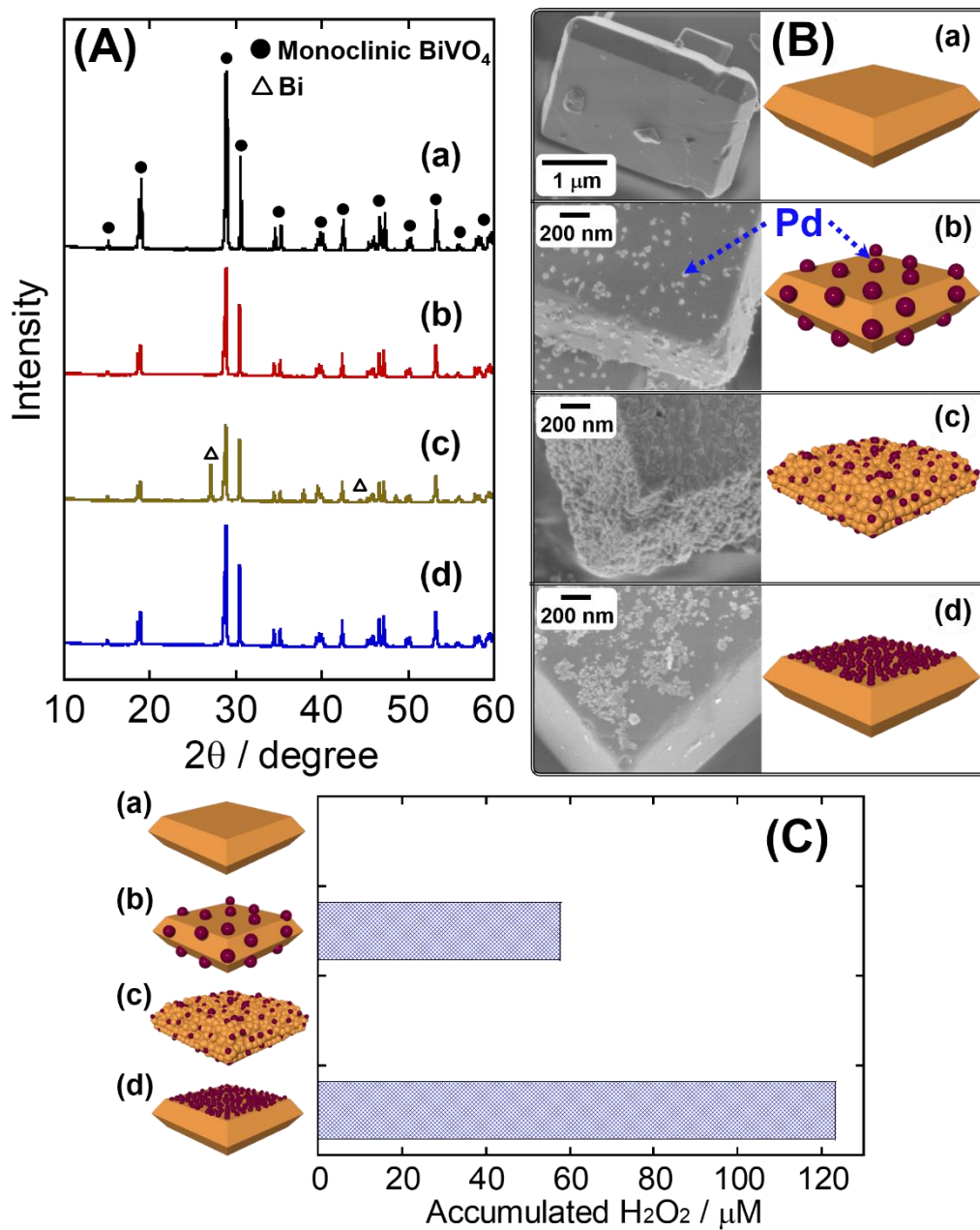
Fig. 3. (A) XRD patterns, (B) SEM images (inset: corresponding Pd-BiVO₄ illustrations), and (C) H₂O₂ production performances of (a) bare BiVO₄ and 1 wt% Pd-BiVO₄ prepared using (b) IMP, (c) DP-CR, and (d) PAD without phosphate addition under visible light (λ > 420 nm) irradiation for 2 h.
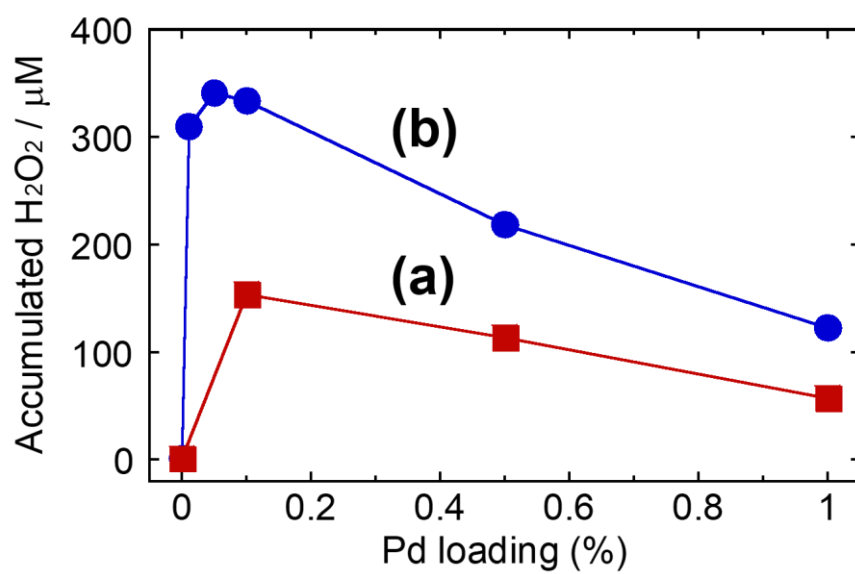
Fig. 4. Effects of Pd loading using (a) IMP and (b) PAD methods (without phosphate) on H_2O_2 production from O_2 in the presence of CH_3OH under visible light ($\lambda > 420$ nm) irradiation for 2 h.
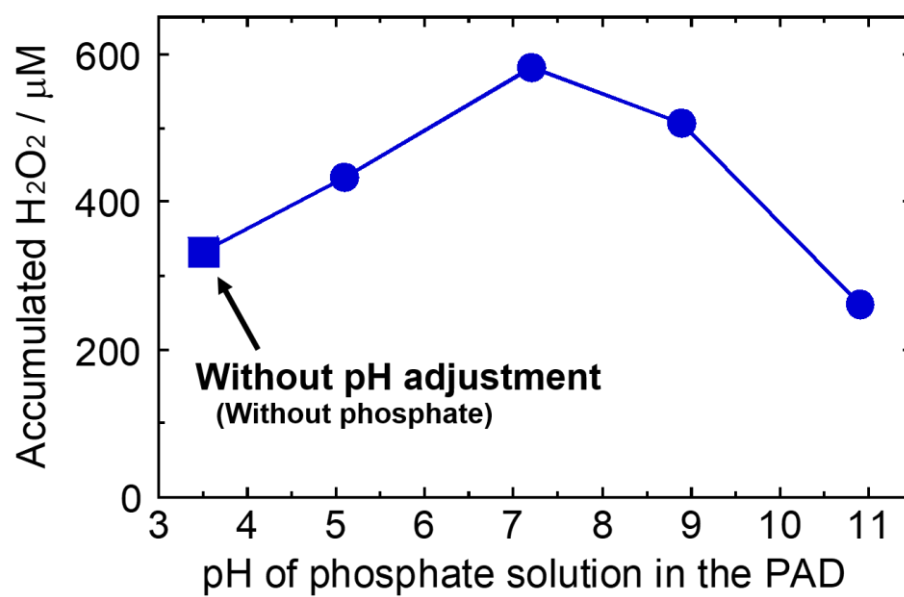
Fig. 5. H_2O_2 production from O_2 in the presence of CH_3OH under visible light ($\lambda > 420$ nm) irradiation for 2 h over 0.1 wt% Pd-BiVO$_4$ prepared using the PAD method with phosphate buffer solutions of different pH.

Sample	Average size (d_{av}) / nm	Abundance rate (%)		
		< 10 nm	10 ~ 20 nm	Others
(a)	24.9	63	25	12
(b)	8.5	77	23	0
(c)	27.4	37	43	20
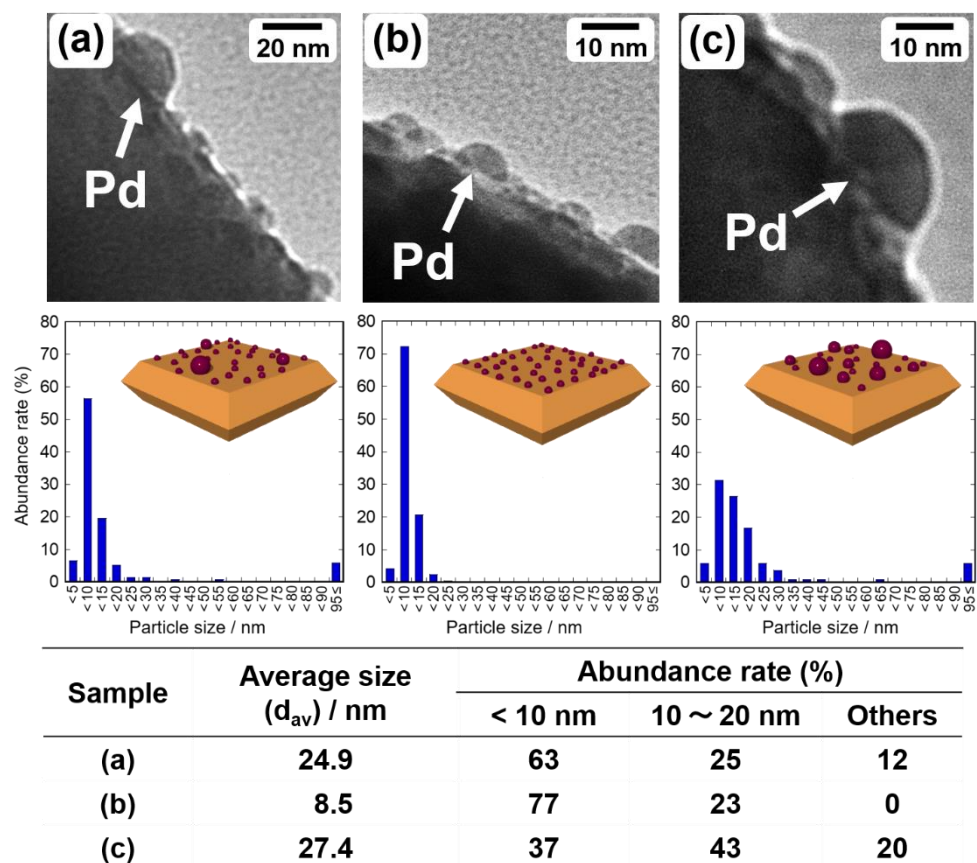
Fig. 6. TEM images, size distributions (insets: NP coverage schematics), and average particle sizes (d_{av}) of Pd NPs of 0.1 wt% Pd-BiVO$_4$ prepared using the PAD method at pH = (a) 3.5 (*i.e.*, without phosphate), (b) 7.2, and (c) 10.9.
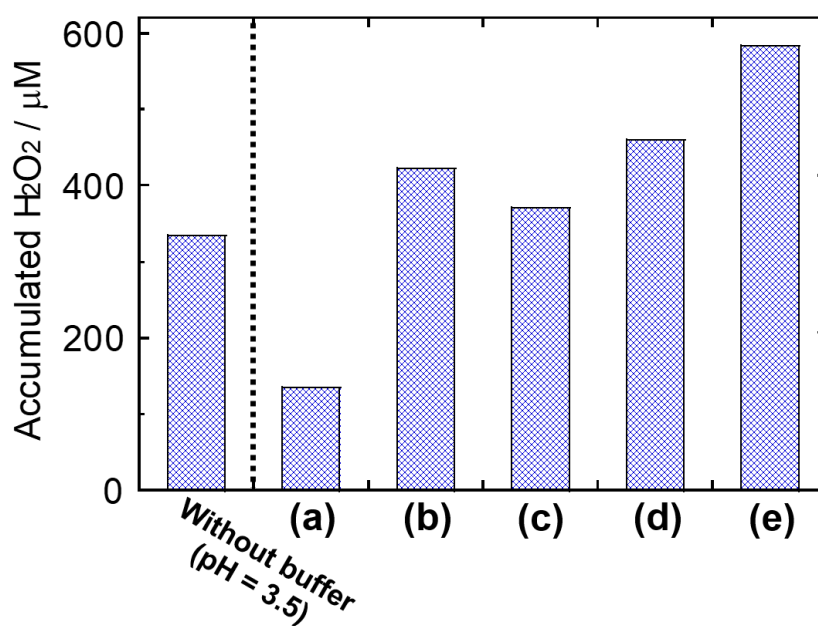
Fig. 7. H$_2$O$_2$ production from O$_2$ in the presence of CH$_3$OH under visible light ($\lambda > 420$ nm) irradiation for 2 h over 0.1 wt% Pd-BiVO$_4$ prepared by PAD at pH = *ca.* 7 using (a) citrate, (b) acetate, (c) carbonate, (d) borate, or (e) phosphate buffer solutions.
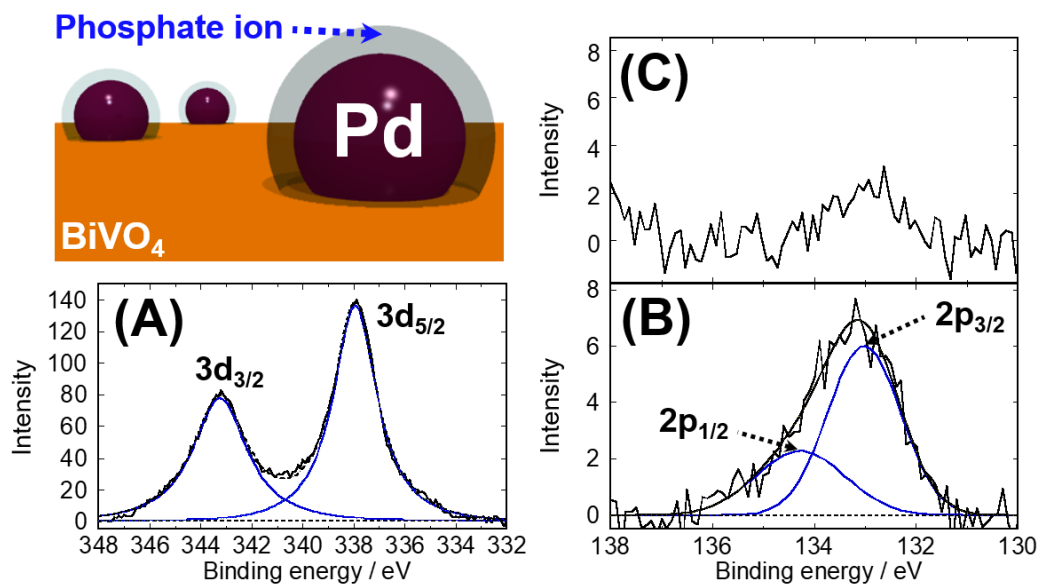
Fig. 8. (A) Pd(3d) and (B) P(2p) XPS spectra of 1.0 wt% Pd-BiVO$_4$ prepared using PAD

at pH = 7.2 in an aqueous phosphate buffer solution, and (C) P(2p) XPS spectrum of

BiVO$_4$ photo-irradiated in an ice bath for 2 h at λ > 300 nm using a 300-W Xe illuminator

in an aqueous phosphate buffer solution adjusted to pH = 7.2 without (NH$_4$)$_2$[PdCl$_4$].
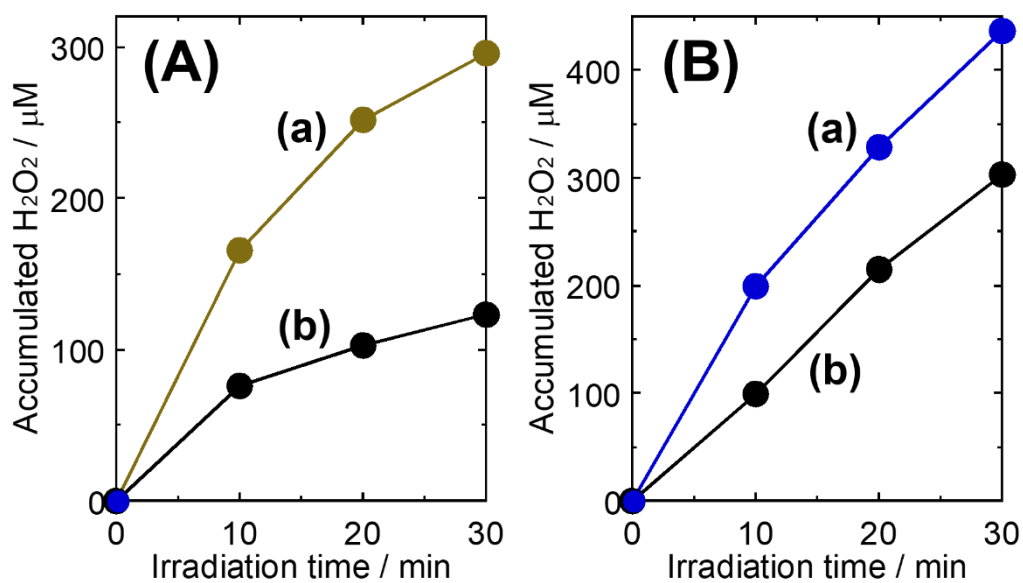
Fig. 9. Comparison of H_2O_2 production from O_2 (a) without or (b) with the initial addition of H_2O_2 (200 μM) in the presence of CH_3OH under visible light ($\lambda > 420$ nm) irradiation over 0.1 wt% Pd-$BiVO_4$ prepared using PAD in aqueous (A) carbonate and (B) phosphate buffer solutions (pH = *ca.* 7).
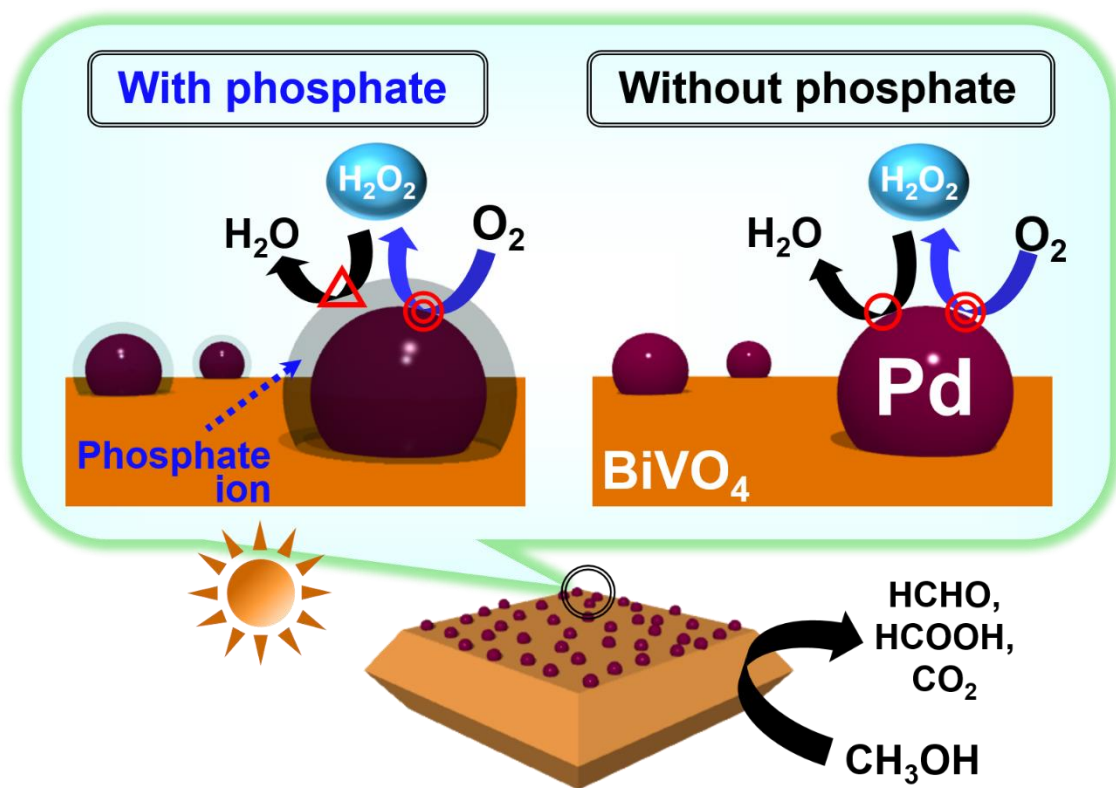
Fig. 10. Proposed mechanism for the effect of phosphate on photocatalytic H_2O_2 production from O_2 in the presence of CH_3OH over Pd-BiVO$_4$ prepared using PAD.